Modeling of ultrafast interferometric three-photon photoemission from a metal surface irradiated with sub-10-fs laser pulses

A. T. Georges* and N. E. Karatzas
Department of Physics, University of Patras, Patras 26500, Greece
(Received 7 December 2007; revised manuscript received 29 January 2008; published 29 February 2008)

We present an effective four-level density matrix model for describing ultrafast interferometric three-photon photoemission (3PPE) from a metal surface. The model accounts for the slow resonant and the fast nonresonant excitation channels through the energy continua, in the presence of energy and phase relaxation of the electronic states. Calculations are presented for the case of a gold surface irradiated with 9.5 fs Ti:sapphire laser pulses, where we find good agreement with recent experimental results for the photocharge vs the time delay between two identical laser subpulses. Numerical results are also presented for the photocurrent densities of the different excitation channels and the photocharge densities vs time delay for various laser pulse widths from 100 down to 2.5 fs (one optical period). It is shown that interferometric 3PPE can be used to measure sub-10-fs laser pulse widths and for extracting lifetimes of conduction electrons.

DOI: 10.1103/PhysRevB.77.085436 PACS number(s): 78.47.J−, 79.60.−i, 42.65.Re, 42.50.Hz

I. INTRODUCTION

Interferometric two-photon photoemission (2PPE) and surface second-harmonic generation (SSHG) have been widely used over the past decade for measuring electron lifetimes and studying ultrafast electron dynamics in metallic surfaces, thin films, and nanoparticles.[1–12] The techniques are based on the use of two identical laser pulses with a relative time delay between them and the measurement of the photoelectrons or the second-harmonic photons as a function of the time delay. In the weak field approximation, the measured signals for both 2PPE and SSHG are proportional to the second-order autocorrelation of the laser pulse, which though is broadened because of the finite electron response (relaxation) time. By fitting the measured correlation curves with calculations for a three-level density matrix model, the lifetimes are extracted. However, as was reported by Weida *et al.*[3] in the case of 2PPE experiments with cesiated copper and 19 fs full width at half maximum (FWHM) laser pulses (herein the FWHM refers to the intensity envelope), the three-level model can predict unphysically fast (in their case, a factor of 3 faster than other methods) energy relaxation times for hot electrons. This is because, for very short femtosecond laser pulses, a simple three-level model cannot describe adequately the actual continuum-continuum transitions that are involved in such processes in metals. They have shown this in a heuristic approach for the case of 13.5 fs laser pulses by calculating the total photocurrent as an incoherent superposition of the contributions from a set of three-level systems with varying one- and two-photon detunings.[4] The calculated correlation curve in the case of the superposition is narrower than that in the case of a simple resonant three-level system, owing to cancellation effects in the sum of the interferograms in the former case. This narrowing effect was later confirmed in simulations with 7.3 fs laser pulses by Timm and Bennemann,[9] who have developed a unified weak field response theory for 2PPE and SSHG that accounts for band to band transitions.

In a recent work,[13] dealing with the effects of electron relaxation on multiple harmonic generation from a gold surface, we found that for laser pulses shorter than the electron relaxation time (~30 fs), a density matrix model with a finite number of levels and realistic relaxation rates could not reproduce experimental interferometric autocorrelation curves. The experiment by Dai *et al.*[14] on SSHG with 18 fs Ti:sapphire laser pulses shows that, despite electron relaxation, the response time of a gold surface autocorrelator is practically the same as for two-photon interband absorption in a GaAsP photodiode. It should be noted here that in the latter case, the intermediate one-photon transitions are far away from resonance, which happens to fall into the semiconductor energy gap, and this makes them very fast. In another recent experiment, Dombi *et al.*[15] have measured nearly the same value for the width of 9.5 fs Ti:sapphire laser pulses using interferometric three-photon photoemission from a gold surface as with interferometric second-harmonic generation in a nonlinear crystal. Although the experimental autocorrelation curves from both the nonlinear crystal and the gold surface exhibit long tails due to different limiting effects, the widths of their central peak show that the response time of gold is nearly as short as that of the crystal, where the nonlinear process is nonresonant. As we concluded in Ref. 13, the only physical explanation for these two interesting experiments[14,15] is that for laser pulses shorter than the electron relaxation times, the contribution of the fast nonresonant channel in the continuum, which is neglected as weak in density matrix models,[1–13] becomes important as the resonant channel becomes slow (relative to the laser pulse width) and less efficient. We should add that this is also the reason for the narrowing effect mentioned earlier, which has been viewed as a consequence of the averaging over the continuum.[4,9] Therefore, in order to describe accurately such processes for laser pulse widths shorter than ~30 fs, a more detailed density matrix model is required for continuum-continuum transitions in metals, in the presence of both energy and phase relaxation for electronic states. It is the purpose of this paper to introduce, for each initial state, an effective $(N+1)$-resonant-level density matrix model for N-photon processes in metals and other media with energy continua, where the nonresonant off-diagonal density matrix

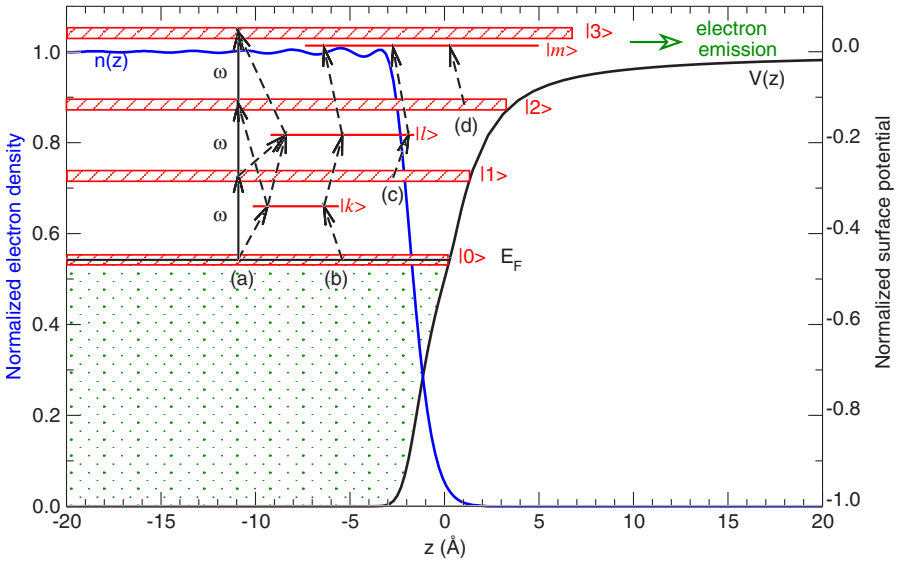

FIG. 1. (Color online) Plot of the model surface potential $V(z)$ (black line) and the electron density $n(z)$ (blue or dark gray) normalized to their respective bulk values. The relevant energy levels for three-photon photoelectron emission are shown in red (light gray). The black arrows show the four different channels: (a) resonant, (b) nonresonant, (c) from the one-, and (d) the two-photon excited states.

elements have been eliminated adiabatically, and the effect of the nonresonant continuum is accounted for by multiphoton transition matrix elements between the resonant states. To illustrate our theoretical approach, in Sec. II, we present the effective four-level density matrix model for describing three-photon photoemission (3PPE) from a metal surface. It is shown that in this case, there are four different channels with different response times. Then, in Sec. III, we present numerical calculations pertaining to the experiment with 9.5 fs laser pulses by Dombi *et al.*,[15] as well as the predictions of the model for shorter and longer pulses.

II. THEORETICAL MODEL

Figure 1 shows the process of 3PPE from a metal surface. As in Ref. 16, we treat the metal surface in the jellium approximation, and in the numerical calculations for gold, we use the same model surface potential as therein. The potential $V(z)$ and the corresponding electron density $n(z)$ are shown normalized to their respective bulk values. The model incorporates the Coulombic fall off of an image potential and the experimental value for the work function, the latter being crucial in determining the order of the multiphoton photoemission process. Since the surface breaks the translational invariance, the momentum is not a good quantum number, and because of the nonperiodic potential, there is only one energy continuum in the jellium model. It should be pointed here that the emphasis in this paper is on the physics of multiphoton surface photoemission and not on the detailed description of the metal surface. Of course, the formalism can be applied to more complex models for the metal surface and to other media with one or more energy continua. The obliquely incident laser beam is assumed to be p polarized, and within our model, multiphoton photoemission is purely a surface effect, which is known from experiments to dominate over the corresponding bulk effect.[15] Note that, in a multiphoton surface effect, there is coupling between the laser electric field component normal to the surface and the electrons in the surface region where $dV/dz \neq 0$, which provides the necessary momentum for the process. The solid line arrows in Fig. 1, starting from an initial state $|0\rangle$ at the Fermi energy E_F, going through the one- and two-photon excited states $|1\rangle$ and $|2\rangle$, and ending at the three-photon excited state $|3\rangle$ above the vacuum level in the positive energy continuum, indicate the resonant excitation channel. This is the channel that is described by the density matrix equations in Ref. 16. Note that, in continuum-continuum transitions, the term resonant refers to energy conserving transitions, while the term nonresonant refers to the nonenergy conserving ones. The dashed line arrows in channel (a) indicate the enhancement of the resonant channel by fast two- and three-photon transitions ($|0\rangle \leftrightarrow |2\rangle$, $|1\rangle \leftrightarrow |3\rangle$, and $|0\rangle \leftrightarrow |3\rangle$) via nonresonant intermediate states, $|k\rangle$ and $|l\rangle$, in the continuum. The dashed line arrows in channel (b) indicate the fast nonresonant 3PPE, those in channel (c) indicate 2PPE from the one-photon excited state, and channel (d) one-photon photoemission from the two-photon excited state. Of the four channels for 3PPE, the slowest is (a) because of energy and phase relaxation in the resonant states. The fastest channel is (b), since the intermediate states are nonresonant and, therefore, its response is instantaneous. The response of channel (c) is the second faster, limited by the lifetime of state $|1\rangle$, while that of channel (d) is the third faster, limited by the lifetime of both states $|1\rangle$ and $|2\rangle$.

In the slowly varying amplitude approximation, which has been shown to give an unambiguous description for pulse durations as short as one carrier period,[17] and given that the skin depth is much less than a free-space wavelength, the z component of the laser electric field can be written as

$$E_z(x,z,t) = \mathcal{E}(t) f(z) e^{i(\omega_c t - k_{cx} x)} + \text{c.c.}, \tag{1}$$

where $\mathcal{E}(t)$ is a slowly varying amplitude, ω_c the central (carrier) frequency, and

$$f(z) \simeq \begin{cases} [e^{ik_{cz}(z-z_0)} + \varrho_c e^{-ik_{cz}(z-z_0)}]\sin\vartheta_i, & z > z_0 \\ \tau_c(1+\varrho_c)\sin\vartheta_t e^{(ik'_{ctz}+k''_{ctz})(z-z_0)}, & z < z_0 \end{cases} \tag{2}$$

gives the z dependence in the Fresnel approximation of transverse fields, with $z_0=0$ being the position of the plane of

reflection in the tail of the electron density. The investigation of the effect of the longitudinal z component inside the metal,[18] on surface 3PPE with ultrafast laser pulses, is outside the scope of this work. In the equations above, $\varrho_c = [n(\omega_c)\cos\vartheta_i - \cos\vartheta_{ct}]/[n(\omega_c)\cos\vartheta_i + \cos\vartheta_{ct}]$ is the amplitude reflection coefficient at the central frequency, with $n(\omega_c)$ being the complex index of refraction of the metal in the bulk, ϑ_i the angle of incidence, and ϑ_{ct} the complex angle of refraction. $\tau_c = \epsilon_0/\epsilon(\omega_c)$ is the amplitude transmission coefficient, with $\epsilon(\omega_c)$ being the dielectric function of the metal. The components of the incident wave vector are $k_{cx} = (\omega_c/c)\sin\vartheta_i$ and $k_{cz} = (\omega_c/c)\cos\vartheta_i$, while the complex z component of the wave vector in the metal is $k_{ctz} = k'_{ctz} - ik''_{ctz} = (\omega_c/c)[\epsilon(\omega_c)/\epsilon_0 - \sin^2\vartheta_i]^{1/2}$. For the dielectric function of the metal, we use a free-electron gas model with damping, $\epsilon(\omega) = \epsilon_0[1 - \omega_p^2/\omega(\omega - i\Gamma_D)]$, with ω_p being the bulk plasma frequency and Γ_D the frequency dependent Drude damping rate. Since the interaction is described in the velocity gauge, it is preferable to specify the amplitude of the vector potential $\mathcal{A}(t)$ and use the relation

$$\mathcal{E}(t) = -i\omega_c \mathcal{A}(t)\left[1 - i\frac{1}{\omega_c \mathcal{A}}\frac{d\mathcal{A}}{dt}\right] \tag{3}$$

to obtain the amplitude of the electric field. Using a Gaussian amplitude, $\mathcal{A}(t) = \mathcal{A}_0 \exp[-2\ln 2(t/\tau_p)^2]$, where τ_p is the FWHM of the pulse, our calculations show that, for pulse durations as short as one optical period, the contribution of the second term in the square brackets on the right hand side (rhs) of the above equation to $\mathrm{Re}[\mathcal{E}(t)e^{i\omega_c t}]$ and its spectrum is small. The FWHM of the energy spectrum in eV for a Gaussian pulse is $\hbar\Delta\omega/e = \hbar e^{-1} 4\ln 2/\tau_p$, and for $\tau_p = 2\pi/\omega_c$, the relative half bandwidth is $\Delta\omega/2\omega_c = \ln 2/\pi = 22\%$.

To describe the coherent interaction between the laser and a medium with an energy continuum that is subject to both energy damping and dephasing, the use of the density matrix formalism is necessary. We begin by discretizing the continuum and, since conduction electrons are localized, we use the normalized Gaussian wave packets $\Phi_i(z)$ of plane wave eigenstates for a more realistic description, as in Ref. 16 where the reader is referred to for more details. In the calculations presented here for gold, the frequency FWHM of the Gaussian electron wave packets is set equal to $D = 4 \times 10^{14}\ \mathrm{s}^{-1}$, which corresponds to an uncertainty in momentum of $\Delta k \simeq 10^{-2} k_F$ and an uncertainty in position of $\Delta z = 1/(2\Delta k) \simeq 40$ Å. The latter satisfies the requirements of semiclassical theory,[19] that the electron wave packets be several lattice constants (4 Å) long, but shorter than the mean free path. The resonant one- and multiphoton transitions are treated strongly, while the nonresonant density matrix elements are eliminated adiabatically. Their effect appears in the equations of motion for the resonant density matrix elements through the multiphoton Rabi frequencies and ionization rates. The density matrix equations that one obtains in this way for the effective four-resonant-level system which describes 3PPE are

$$\frac{d}{dt}\sigma_{00} = \mathrm{Im}[\Omega_{01}^{(1)*}\sigma_{01}^{(1)}] + \mathrm{Im}[\Omega_{02}^{(2)*}\sigma_{02}^{(2)}] + \mathrm{Im}[\Omega_{03}^{(3)*}\sigma_{03}^{(3)}] + \gamma_1^{nr}\sigma_{11} + \gamma_2^{nr}\sigma_{22} + \gamma_3^{nr}\sigma_{33} - \gamma_0^{ee}\sigma_{00} - \mathrm{Re}[\gamma_{01}^{ee}\sigma_{01}^{(1)}] - \mathrm{Re}[\gamma_{02}^{ee}\sigma_{02}^{(2)}], \tag{4}$$

$$\left[\frac{d}{dt} + \frac{1}{2}\Gamma_{01}\right]\sigma_{01}^{(1)} = -\frac{i}{2}(\sigma_{00} - \sigma_{11})\Omega_{01}^{(1)} - \frac{i}{2}\sigma_{02}^{(2)}\Omega_{12}^{(1)*} - \frac{i}{2}\sigma_{03}^{(3)}\Omega_{13}^{(2)*}, \tag{5}$$

$$\left[\frac{d}{dt} + \gamma_1\right]\sigma_{11} = -\mathrm{Im}[\Omega_{01}^{(1)*}\sigma_{01}^{(1)}] + \mathrm{Im}[\Omega_{12}^{(1)*}\sigma_{12}^{(1)}] + \mathrm{Im}[\Omega_{13}^{(2)*}\sigma_{13}^{(2)}], \tag{6}$$

$$\left[\frac{d}{dt} + \frac{1}{2}\Gamma_{02}\right]\sigma_{02}^{(2)} = -\frac{i}{2}(\sigma_{00} - \sigma_{22})\Omega_{02}^{(2)} - \frac{i}{2}\sigma_{01}^{(1)}\Omega_{12}^{(1)} + \frac{i}{2}\Omega_{01}^{(1)}\sigma_{12}^{(1)} - \frac{i}{2}\sigma_{03}^{(3)}\Omega_{23}^{(1)*}, \tag{7}$$

$$\left[\frac{d}{dt} + \frac{1}{2}\Gamma_{12}\right]\sigma_{12}^{(1)} = -\frac{i}{2}(\sigma_{11} - \sigma_{22})\Omega_{12}^{(1)} - \frac{i}{2}\sigma_{13}^{(2)}\Omega_{23}^{(1)*} + \frac{i}{2}\Omega_{01}^{(1)*}\sigma_{02}^{(2)}, \tag{8}$$

$$\left[\frac{d}{dt} + \gamma_2\right]\sigma_{22} = -\mathrm{Im}[\Omega_{12}^{(1)*}\sigma_{12}^{(1)}] + \mathrm{Im}[\Omega_{23}^{(1)*}\sigma_{23}^{(1)}] - \mathrm{Im}[\Omega_{02}^{(2)*}\sigma_{02}^{(2)}], \tag{9}$$

$$\left[\frac{d}{dt} + \frac{1}{2}\Gamma_{03}\right]\sigma_{03}^{(3)} = -\frac{i}{2}(\sigma_{00} - \sigma_{33})\Omega_{03}^{(3)} - \frac{i}{2}\sigma_{02}^{(2)}\Omega_{23}^{(1)} + \frac{i}{2}\Omega_{01}^{(1)}\sigma_{13}^{(2)} - \frac{i}{2}\sigma_{01}^{(1)}\Omega_{13}^{(2)} + \frac{i}{2}\Omega_{02}^{(2)}\sigma_{23}^{(1)}, \tag{10}$$

$$\left[\frac{d}{dt} + \frac{1}{2}\Gamma_{13}\right]\sigma_{13}^{(2)} = -\frac{i}{2}(\sigma_{11} - \sigma_{33})\Omega_{13}^{(2)} - \frac{i}{2}\sigma_{12}^{(1)}\Omega_{23}^{(1)} + \frac{i}{2}\Omega_{12}^{(1)}\sigma_{23}^{(1)} + \frac{i}{2}\Omega_{01}^{(1)*}\sigma_{03}^{(3)}, \tag{11}$$

$$\left[\frac{d}{dt} + \frac{1}{2}\Gamma_{23}\right]\sigma_{23}^{(1)} = -\frac{i}{2}(\sigma_{22} - \sigma_{33})\Omega_{23}^{(1)} + \frac{i}{2}\Omega_{12}^{(1)*}\sigma_{13}^{(2)} + \frac{i}{2}\Omega_{02}^{(2)*}\sigma_{03}^{(3)}, \tag{12}$$

$$\left[\frac{d}{dt}+\gamma_3\right]\sigma_{33}=-\mathrm{Im}[\Omega_{23}^{(1)*}\sigma_{23}^{(1)}]-\mathrm{Im}[\Omega_{13}^{(2)*}\sigma_{13}^{(2)}]-\mathrm{Im}[\Omega_{03}^{(3)*}\sigma_{03}^{(3)}], \quad (13)$$

where σ_{ii} and $\sigma_{ij}^{(N)}=\rho_{ij}e^{-iN(\omega_c t-k_x x)}$ are the slowly varying diagonal and off-diagonal matrix elements of the density matrix ρ in the rotating wave approximation, respectively. In the definition of the latter, the superscript (N) refers to the N-photon resonance of the element with the central frequency of the laser spectrum. We should point out here that the expansion of the off-diagonal density matrix elements, for media with energy continua, in harmonics of the central laser frequency should hold for pulse widths down to one optical cycle ($\Delta\omega/2\omega_c=22\%$). Two- or four-photon stepwise resonant excitation by photons in the wings of the laser spectrum would be slow like the resonant 3PPE channel (a) and weaker compared to it. Moreover, these processes would be much less efficient than the fast nonresonant channel (b), which for ultrashort pulses becomes the dominant channel. In the special case, as in Ref. 20, where $3\hbar\omega_c$ is nearly equal to the 5 eV work function of the metal and both 3PPE and four-photon photoemission take place, the excitation ladder in our model should be extended to one more resonant state, $|4\rangle$. Then, one should calculate the three- and four-photon photocurrent densities, whose sum follows an I^x power law, with x between 3 and 4, as in the particular experiment.

The one-photon Rabi (interaction) frequencies are defined as

$$\Omega_{i,i+1}^{(1)}=2\hbar^{-1}\langle\Phi_i|\mathcal{H}^{(1)}|\Phi_{i+1}\rangle, \quad (14)$$

where $\mathcal{H}^{(1)}=-(e/m)\mathcal{A}(t)f(z)p_z$ is the component of the interaction Hamiltonian first order in the amplitude of the vector potential and p_z the z component of the electron momentum. The two-photon Rabi frequencies are defined as

$$\Omega_{i,i+2}^{(2)}=-\frac{1}{2}\sum_{k\neq i+1}\frac{\Omega_{ik}^{(1)}\Omega_{k,i+2}^{(1)}}{(\omega_c-\omega_{i+2,k})}+\mathcal{V}_{i,i+2}^{(2)}, \quad (15)$$

where $\mathcal{V}_{i,i+2}^{(2)}=2\hbar^{-1}\langle\Phi_i|\mathcal{H}^{(2)}|\Phi_{i+2}\rangle$, with $\mathcal{H}^{(2)}=(e^2/2m)\mathcal{A}^2(t)f^2(z)$ being the component of the interaction Hamiltonian second order in $\mathcal{A}(t)$. Likewise, the three-photon Rabi frequency $\Omega_{03}^{(3)}$ is given by

$$\Omega_{03}^{(3)}=\frac{1}{4}\sum_{k\neq 1,l\neq 2}\frac{\Omega_{0k}^{(1)}\Omega_{kl}^{(1)}\Omega_{l3}^{(1)}}{(2\omega_c-\omega_{l0})(\omega_c-\omega_{k0})}-\frac{1}{2}\sum_{k\neq 1}\frac{\Omega_{0k}^{(1)}\mathcal{V}_{k3}^{(2)}}{(\omega_c-\omega_{k0})}-\frac{1}{2}\sum_{l\neq 2}\frac{\mathcal{V}_{0l}^{(2)}\Omega_{l3}^{(1)}}{(2\omega_c-\omega_{l0})}. \quad (16)$$

At this stage, it should be pointed out that the improvement over previous density matrix treatments of laser-metal interaction[1–13,16] lies in the inclusion of the nonresonant continuum, whose effect is taken into account by the terms with summation over $|k\rangle$ and/or $|l\rangle$ in Eqs. (15) and (16). These terms are obtained by adiabatic elimination of the nonresonant density matrix elements, such as $\sigma_{0k}^{(1)}$, $\sigma_{kl}^{(1)}$, $\sigma_{0l}^{(2)}$, $\sigma_{0m}^{(3)}$, etc. In the numerical evaluation of the two- and three-photon Rabi frequencies, the symbolic sum over, for example, the intermediate $|l\rangle$ wave packet states is replaced by $\int[\cdots]g_w(\omega_l)d\omega_l$, where $g_w(\omega_l)=g(\omega_l)/\mathcal{N}_l$ is the density of the wave packet states. In the relation for the latter, $g(\omega_l)=L_z m/(2\pi\hbar k_z)$ is the one dimensional density of eigenstates, with L_z being a normalization length and k_z the z component of the wave vector for an electron state with energy $\hbar\omega_l$. The division by $\mathcal{N}_l$, which is the effective number of eigenstates within a wave packet state,[16] is required for renormalization of the density of states.

The decay rate of the σ_{jj} density matrix element, $\gamma_j=\gamma_j^{nr}+\gamma_j^{ee}$, is the sum of the nonradiative energy decay rate (γ_j^{nr}) and the electron emission rate (γ_j^{ee}) from the $|j\rangle$ state. Note that the spontaneous decay rate of the excited states is neglected because it is many orders of magnitude smaller than the nonradiative. For the latter, we use the relation $\gamma_j^{nr}=\Gamma_D(j\omega_c)$, where $\Gamma_D(j\omega_c)$ is a Drude relaxation rate for a state that is j photons above the Fermi level, and we use the empirical formula $\Gamma_D(j\omega_c)=[0.3+0.01(j\hbar\omega_c)^2]\times 10^{14}$ s^{-1}, with the photon energy in eV, which was obtained in Ref. 16 by fitting experimental results. The functional form for $\Gamma_D(j\omega_c)$ is the same as that in Ref. 21 for electron phonon and impurity scattering in noble metals for the case $\omega_c\gg\Gamma_D$. The energy relaxation time (γ_j^{-1}) found using this formula and the corresponding value for γ_j^{ee} varies from about 33 fs at 1 eV to 5 fs at 6 eV above the Fermi energy. We should mention that the electron lifetimes, $\tau\simeq 2(E_F/\hbar\omega)^2$ fs, for gold predicted by the Fermi liquid theory,[22] at these two energies are about 60 and 2 fs, respectively. However, Fermi liquid theory accounts only for electron-electron elastic and inelastic scatterings, and one cannot separate the energy relaxation rate from the dephasing rate. For the off-diagonal σ_{ij} matrix element, the relaxation rate is set equal to $\frac{1}{2}\Gamma_{ij}=\frac{1}{2}(\gamma_i^{ee}+\gamma_j^{ee})+\Gamma_D(j\omega_c)$ with $j>i$. Since $\Gamma_D(j\omega_c)>\frac{1}{2}[\Gamma_D(i\omega_c)+\Gamma_D(j\omega_c)]$, our relation for Γ_{ij} allows for some contribution from phase relaxation or elastic collisions to the decay rate of coherence.

The nonresonant three-photon electron emission rate from state $|0\rangle$, γ_0^{ee}, which corresponds to channel (b) and arises naturally in Eq. (4) from the adiabatic elimination of $\sigma_{0m}^{(3)}$ in a $\mathrm{Im}[\Sigma_{m\neq 3}\Omega_{0m}^{(3)*}\sigma_{0m}^{(3)}]$ term in that equation, is given by

$$\gamma_0^{ee}=\frac{1}{2}\sum_{m\neq 3}\frac{\Gamma_{0m}/2}{(3\omega_c-\omega_{m0})^2+(\Gamma_{0m}/2)^2}|\Omega_{0m}^{(3)}|^2=\frac{\pi}{2}|\Omega_{03}^{(3)}|^2 g_w(\omega_0+3\omega_c). \quad (17)$$

The final result is obtained when we change the summation over m to integration over ω_{m0}, and in the limit of $\Gamma_{0m}\to 0$ replace the Lorentzian by $\pi\delta(\omega_{m0}-3\omega_c)$. In a similar manner, it can be shown that the nonresonant two-photon electron emission rate from state $|1\rangle$ is given by

$$\gamma_1^{ee}=\frac{\pi}{2}|\Omega_{13}^{(2)}|^2 g_w(\omega_0+3\omega_c), \quad (18)$$

while the one-photon electron emission rate from state $|2\rangle$ by

$$\gamma_2^{ee} = \frac{\pi}{2}|\Omega_{23}^{(1)}|^2 g_w(\omega_0 + 3\omega_c). \tag{19}$$

The complex cross emission rates appearing in the terms $\mathrm{Re}[\gamma_{01}^{ee}\sigma_{01}^{(1)}]$ and $\mathrm{Re}[\gamma_{02}^{ee}\sigma_{02}^{(2)}]$ on the rhs of Eq. (4) are given by

$$\gamma_{01}^{ee} = \frac{\pi}{2}\Omega_{13}^{(2)}\Omega_{03}^{(3)*} g_w(\omega_0 + 3\omega_c) \tag{20}$$

and

$$\gamma_{02}^{ee} = \frac{\pi}{2}\Omega_{23}^{(1)}\Omega_{03}^{(3)*} g_w(\omega_0 + 3\omega_c). \tag{21}$$

These two rates account for the interference between the nonresonant electron emission channels from states $|0\rangle$, $|1\rangle$, and $|2\rangle$, which depends on the coherence between the channels through the nondiagonal density matrix elements $\sigma_{01}^{(1)}$ and $\sigma_{02}^{(2)}$. For the electron wave packet state $|3\rangle$ which lies above the vacuum level, the electron emission rate is

$$\gamma_3^{ee} = \frac{2}{\pi}\int_{\omega_{thr}}^{\infty} \frac{k_z\kappa_z}{(k_z+\kappa_z)^2} G_3(\omega_\alpha) d\omega_\alpha, \tag{22}$$

where k_z and κ_z are the electron wave vectors in the bulk and far outside the metal, respectively, $\hbar\omega_{thr}=V_0$ is the threshold energy for electron emission, and $G_3(\omega_\alpha)=\exp[-4\ln 2(\omega_\alpha-\omega_3)^2/D^2]$ the Gaussian probability distribution for the wave packet.[16] This emission rate is found by multiplying the incident probability current for an eigenstate $[\hbar k_z/(mL_z)]$, the probability for transmission over the surface potential $[4k_z\kappa_z/(k_z+\kappa_z)^2]$, the probability distribution $G_3(\omega_\alpha)$, the density of states $[g(\omega)=L_z m/(2\pi\hbar k_z)]$, and integrating over ω_α. Note that unlike the electron emission rates from the bound states, the emission rate from the above threshold state is independent of the laser intensity. Our calculations show that $\gamma_3^{ee}=3.86\times10^{13}\ \mathrm{s}^{-1}$, while at a laser intensity of $10^{11}\ \mathrm{W/cm^2}$, the other rates are $\gamma_0^{ee}=1.35\times10^7$, $\gamma_1^{ee}=3.3\times10^{10}$, $\gamma_2^{ee}=3.3\times10^{12}$, $|\gamma_{01}^{ee}|=6.6\times10^8$, and $|\gamma_{02}^{ee}|=6.7\times10^9\ \mathrm{s}^{-1}$.

The probability current for 3PPE is given by

$$\begin{aligned}\frac{dP_3}{dt} &= -\frac{d}{dt}\sum_{i=0}^{3}\sigma_{ii} \\ &= \gamma_0^{ee}\sigma_{00} + \gamma_1^{ee}\sigma_{11} + \gamma_2^{ee}\sigma_{22} + \gamma_3^{ee}\sigma_{33} \\ &\quad + \mathrm{Re}[\gamma_{01}^{ee}\sigma_{01}^{(1)}] + \mathrm{Re}[\gamma_{02}^{ee}\sigma_{02}^{(2)}],\end{aligned} \tag{23}$$

and the corresponding current density is calculated from the relation

$$J_3(t) = \delta_s\frac{1}{4\pi^3}\int k_i^2 dk_i \int d\Omega_{k_i} P_{FD}(k_i)\left[e\frac{d}{dt}P_3(t)\right]_{k_i,\Omega_i}, \tag{24}$$

where $\delta_s=1/2k''_{ctz}$ is the skin depth for the field intensity in the metal, e the electron charge, and $P_{FD}(k_i)$ the Fermi–Dirac distribution. The two spin states are taken into account in the density of states, and the integration is over the Fermi sphere, with k_i and Ω_i being the initial electron wavenumber and solid angle.

For measuring autocorrelations, the laser pulse is split into two equal subpulses with a variable time delay τ between them, and thus the following substitution is made in Eqs. (14)–(21) for the electric field (vector potential) amplitude,

$$\mathcal{E}(t) \to \frac{1}{2}[\mathcal{E}(t) + \mathcal{E}(t-\tau)e^{-i\omega_c\tau}]. \tag{25}$$

This makes the photocurrent density a function of both t and τ, and the total photocharge density produced in 3PPE by the two subpulses is

$$Q_3(\tau) = \int_{-\infty}^{\infty} J_3(t,\tau)dt. \tag{26}$$

It is obvious that since all channels for 3PPE are of third order in the intensity of the field as given by relation (25), $Q_3(\tau)$ is proportional to a convolution of the third-order autocorrelation of the laser pulse with the response function of the metal surface. The normalized convoluted third-order autocorrelation is defined as

$$g^{(3)}(\tau) = \frac{Q_3(\tau)}{Q_3(\infty)}. \tag{27}$$

The ideal third-order autocorrelation of the laser pulse is reproduced by the photocharge from the nonresonant channel (b), whose response is instantaneous. For a Gaussian laser field amplitude $\mathcal{E}(t)=\mathcal{E}_0 e^{-t^2/2T^2}$, where $T=\tau_p/\sqrt{4\ln 2}$, the exact third-order autocorrelation is[13]

$$\begin{aligned}g_{ideal}^{(3)}(\tau) &= 1 + 9e^{-2\tau^2/3T^2} + [6e^{-5\tau^2/12T^2} + 9e^{-3\tau^2/4T^2}]\cos(\omega_c\tau) \\ &\quad + 6e^{-2\tau^2/3T^2}\cos(2\omega_c\tau) + e^{-3\tau^2/4T^2}\cos(3\omega_c\tau),\end{aligned} \tag{28}$$

which has a peak to background ratio of 32:1 and a FWHM of $1.253\tau_p$.

III. DISCUSSION OF NUMERICAL RESULTS

Calculations have been carried out for 3PPE from a gold surface using the parameters from the experiment in Ref. 15: work function for polycrystalline gold $W=4.6$ eV, laser wavelength 750 nm ($\hbar\omega=1.653$ eV), and angle of incidence for the laser beam $\vartheta_i=80°$. The Fermi energy for gold is $E_F=5.51$ eV, the electron density $N_e=5.9\times10^{22}\ \mathrm{electrons/cm^3}$, and the skin depth has been calculated to be $\delta_s=110$ Å. The values used for the nonradiative relaxation rates of the density matrix elements are given in the previous section. Gaussian laser pulses with $10^{11}\ \mathrm{W/cm^2}$ peak intensity and various pulse widths from 100 down to 2.5 fs were used in the calculations.

We start the presentation of our numerical results from the case of 9.5 fs pulse width, for which there are experimental results.[15] Figure 2 shows the relative interferometric three-photon photocharge density (red or light gray line) as a function of the time delay between the two laser subpulses. The absolute peak photocharge density is 4.5 $\mathrm{pC/cm^2}$, which for

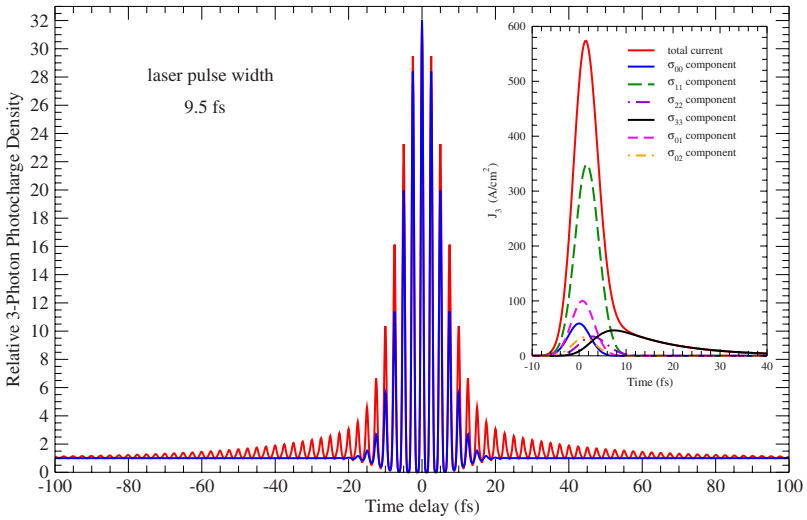

FIG. 2. (Color online) Plot of the relative interferometric three-photon photocharge density vs the time delay between two 9.5 fs laser subpulses of 10^{11} W/cm^2 combined peak intensity. The red (or light gray) curve is for the total photocharge, while the blue (or dark gray) is for the photocharge from the nonresonant channel (b), which gives the exact third-order autocorrelation of the laser pulse. The inset shows the current density vs time for zero time delay from channel: (a) (black line), (b) (blue or dark gray line), (c) (green long dashed line), (d) (violet dash dotted line), interference $\propto\sigma_{01}$ term (magenta short dashed line), interference $\propto\sigma_{02}$ term (orange dash double dotted line), and the total current density (red or light gray).

a laser spot diameter $d_s=7$ μm corresponds to about ten photoelectrons per pulse (the number of electrons in the $\pi d_s^2\delta_s/4$ interaction volume is about 2.5×10^{10}). Although there is no experimental value for the number of photoelectrons in this case, in a related previous work, this number was estimated to be of the order of one photoelectron per pulse.[20] Superimposed (blue or dark gray line) is the photocharge density from the fast nonresonant channel (b) alone, which reproduces the ideal third-order autocorrelation given by Eq. (27). Both curves exhibit the 32:1 peak to background ratio, which is characteristic of third-order interferometric autocorrelations. This feature for the total photocharge density indicates that no saturation effects have set in at 10^{11} W/cm^2 peak laser intensity. Indeed, our calculations show that for a 9.5 fs pulse width, the peak population of the one-photon excited state is only $\sigma_{11}\simeq3.2\times10^{-3}$. The FWHM of the curve for the total photocharge density is about 14.5 fs, which is in good agreement with the experimental results in Fig. 5 of Ref. 15. This width is larger than the 11.9 fs width of the ideal third-order autocorrelation by about 22%. Note that the optical period for a central wavelength of 750 nm is 2.5 fs, and since this equals the spacing of the spikes in the interferogram, the time delay axis in the experimental curves by Dombi *et al.*[15] should be multiplied by a factor of 2. The calculated interferogram for the total photocharge density exhibits, like the experimental one, long wings that extend as far as ±60 fs. The pinchlike feature at about $\tau=\pm17.5$ fs in the experimental curve seems to be caused by a beating between the two main peak frequencies in the actual laser spectrum, which differs substantially from a Gaussian spectrum. The inset in the figure shows the time dependence of the current density from the different channels and the two interference terms, in the case of zero time delay. As can be seen, for a 9.5 fs pulse width, the peak total current is delayed by 1.5 fs relative to the laser peak, and the main contribution (60%) comes from channel (c), 2PPE from the one-photon excited state, a 10% comes from the fast channel (b), and the interference between these two channels adds another 17%. Apparently, the broadening and the long wings of the autocorrelation arise from the electron population that the second laser subpulse finds in the one-photon excited state with the ~30 fs lifetime.

The following two figures demonstrate that the response time of a gold surface 3PPE autocorrelator improves for shorter laser pulse widths. Figure 3 shows the results of calculations for a 4 fs laser pulse. As seen in the inset, in this case, channel (c) contributes only 36% of the total current density, the fast nonresonant channel (b) 31.5%, and the interference term because of their mutual coherence adds another 23%. Even though the contribution of channel (c) is reduced, the electron population in the one-photon excited state still causes long wings in the autocorrelation. The time delay of the peak current density relative to the laser pulse is only 0.4 fs, and the FWHM of the total interferometric photocharge is 5.8 fs, which is 16% larger than the 5.012 fs width of the ideal autocorrelation. Unlike interferometric techniques based on second-harmonic generation in nonlinear crystals, which are known to underestimate the laser pulse width for sub-10-fs pulses because of group velocity dispersion and phase-matching bandwidth limitations,[23–25] a 3PPE gold surface autocorrelator tends to overestimate the laser pulse width. This is due to the contribution of resonant excitation in 3PPE which, though, diminishes as the pulse decreases below 10 fs. In contrast, phase-matching bandwidth limitations in a nonlinear crystal autocorrelator worsen as the pulse width decreases below 10 fs, and the spectral bandwidth of the pulse increases. Figure 4 shows the results of calculations for a 2.5 fs (one optical cycle) Gaussian laser pulse. In this case, the fast nonresonant channel (b) contributes about 47% of the total current density, channel (c) about 23%, and their interference term about 23.5%. Comparing the insets in Figs. 2–4, we see that the peak current density from the instantaneous nonresonant channel (b) is as expected the same, about 60 A/cm^2, for all three pulse widths. The other channels for 3PPE have one, two, or three resonant steps that have a finite response time, and thus their peak current density depends on the pulse duration. The time delay of the peak current density relative to the laser pulse is only 0.125 fs, and the FWHM of the total interferometric photocharge is 3.42 fs, which is 9% larger than the 3.13 fs width of the ideal autocorrelation.

We should point out here that interferometric 3PPE using 2–3 fs laser pulses could be used to look for evidence of the preasymptotic non-Markovian decay of electronic states,

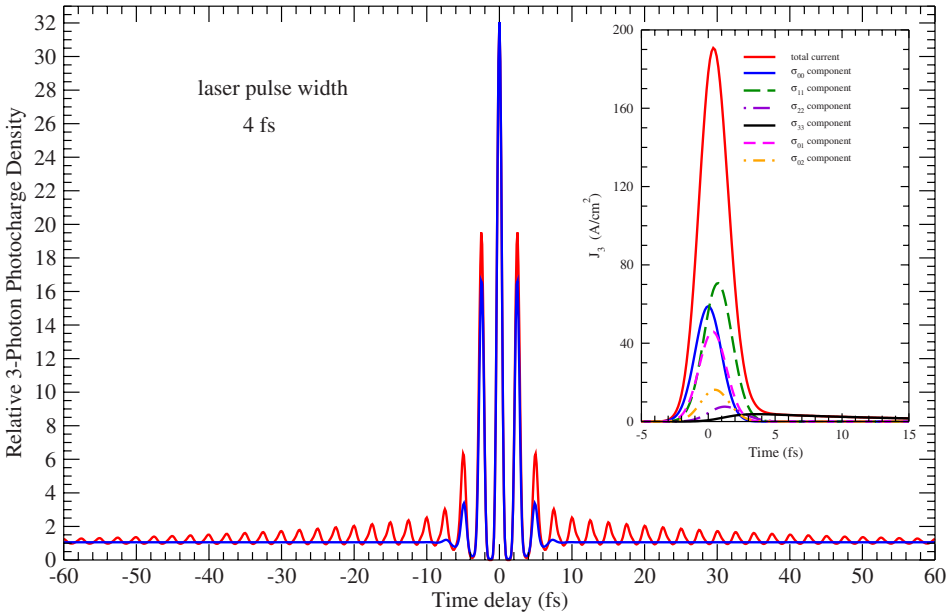

FIG. 3. (Color online) Same as Fig. 2, but for a 4 fs laser pulse width.

which has been predicted[26] to occur in the $0<\tau<2$ fs time range. The signs of preasymptotic behavior should be visible for short time delays when comparing the measured autocorrelation with a Markovian model calculation like the ones presented in this paper. On a different issue, we should also point out that in the rotating wave approximation (RWA) there is no dependence of the photocurrent density on the carrier-envelope phase.[15] If in Eq. (1) for the laser field we replace $e^{i\omega_c t}$ by $e^{i(\omega_c t+\phi_0)}$, where ϕ_0 is a constant phase, the equations of motion for the slowly varying density matrix elements remain invariant. Hence, in the RWA, the excitation step in surface multiphoton electron photoemission does not depend on whether the normal to the surface electric field component points into or out of the metal surface. However, calculations carried out without making the RWA show a very weak modulation in the photocharge vs ϕ_0 curve with a period of π. This modulation is caused by the antiresonant terms, and it has the same period as that predicted in strongly driven two-level systems.[27] It appears, therefore, that the very small (of the order of 10^{-4}) depth of modulation in the photocharge vs ϕ_0 curve, but with a period of 2π, which was reported in Ref. 20 for few cycle laser pulses, is of different origin and must be due to a weak electron transport effect that is not taken into account in our model. A similar weak modulation with a 2π period appears in the photoelectron angular distribution in above threshold ionization of atoms,[28] and it is due to the asymmetric steering of the photoelectrons by the laser field in few-cycle pulses.

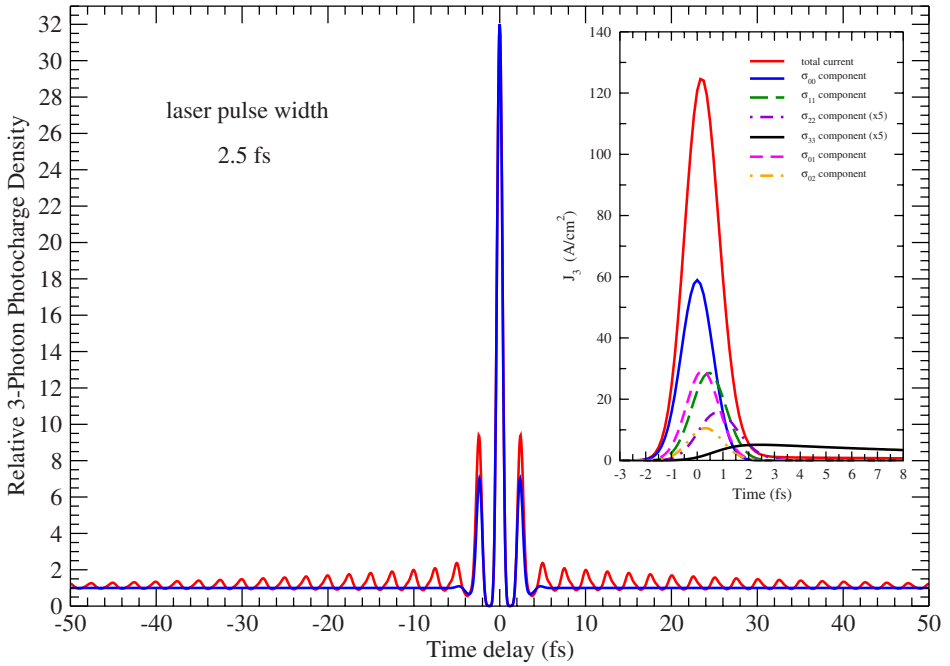

FIG. 4. (Color online) Same as Fig. 2, but for a 2.5 fs laser pulse width.

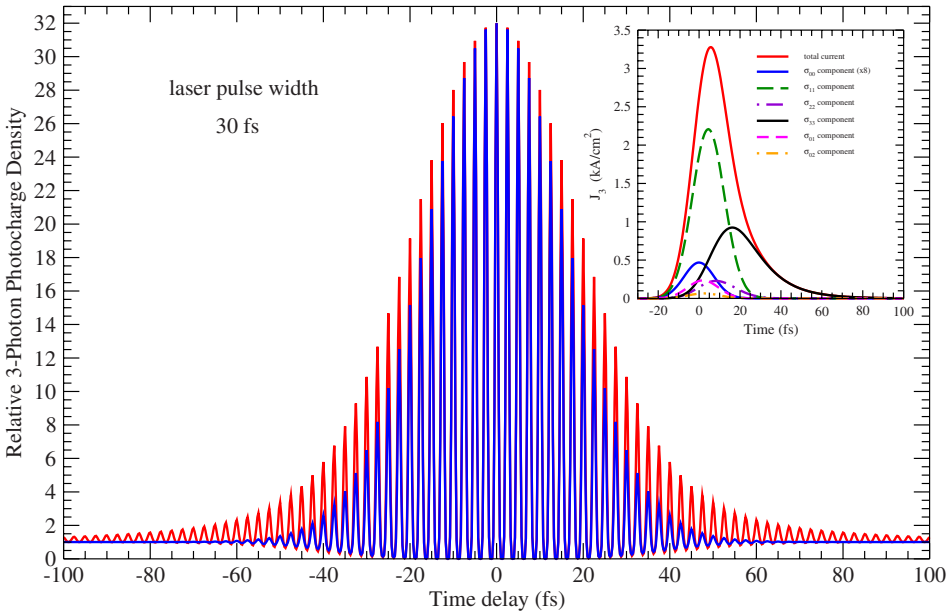

FIG. 5. (Color online) Same as Fig. 2, but for a 30 fs laser pulse width.

The last two figures present 3PPE with long laser pulses. Figure 5 shows the results of calculations for a 30 fs laser pulse, which is of the same duration as the lifetime of the one-photon excited state. In this case, the contribution of channel (c) to the total peak current density is 67%, while that of the slow resonant channel (a) has increased to 27%, from only 7% for a 9.5 fs pulse width. The time delay of the 3.3 kA/cm^2 peak total current density relative to the laser peak is about 5.5 fs, and the FWHM of the total photocharge vs time delay is 45.5 fs, about 21% larger than that of the ideal autocorrelation. Lastly, Fig. 6 shows the results of calculations for a 100 fs laser pulse. For this large pulse width, the peak population of the one-photon excited state becomes a factor of 10 larger than its value in the 9.5 fs case. Also, the contribution of channel (c) drops to 52%, while that of channel (a) increases to 41%. The time delay of the 14.5 kA/cm^2 peak total current density is 17 fs, while the FWHM of the autocorrelation is 137.5 fs, which is about 10% larger that the width of the ideal one. Calculations with longer pulse durations show that, for moderate laser intensities, the resonant channel (a) becomes the dominant one. This justifies the stepwise excitation model for surface multiphoton photoemission with long laser pulses ($\tau_p > 100$ fs), which was introduced in an earlier work.[29] In this case, one can eliminate adiabatically the off-diagonal density matrix elements in Eqs. (3)–(12) and thus obtain rate equations for the populations of the resonant electronic states.[7,11,29] We conclude that in order to have less than 10% error in the measurement of the laser pulse width using a 3PPE gold surface autocorrelator, the pulse width must satisfy the relation $3 \geqslant \tau_p \geqslant 100$ fs. On the other hand, for extracting an electron lifetime that is estimated to be about 30 fs, the laser pulse duration must be in

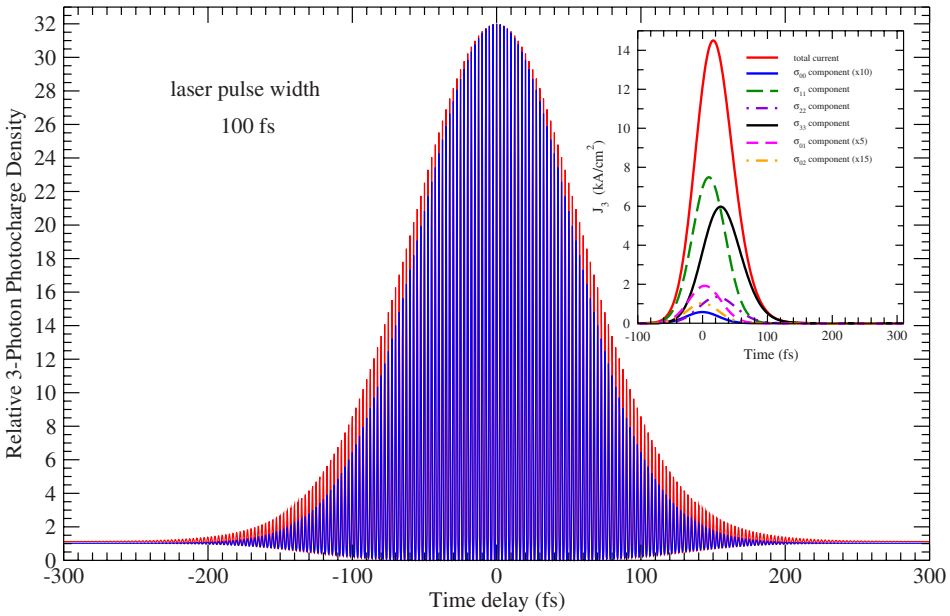

FIG. 6. (Color online) Same as Fig. 2, but for a 100 fs laser pulse width.

the range of $10 < \tau_p < 30$ fs, where the broadening of the third-order autocorrelation is largest and the fitting is easier.

IV. CONCLUSIONS

We have presented an effective four-resonant-level density matrix model for describing ultrafast interferometric three-photon photoemission from media with continuum-continuum transitions, such as metallic surfaces and thin films. The model accounts for the effect of the nonresonant continuum by multiphoton transition matrix elements between the four resonant levels. These matrix elements provide fast nonresonant excitation channels in addition to the resonant stepwise channel, which is slow because of energy and phase relaxation. The need for such a treatment in systems with broadened bands or continua was pointed out by Weida *et al.*,[4] in relation to ultrafast interferometric 2PPE for extracting electron lifetimes. The present work deals with this problem. Our calculations show how important it is to take into account the nonresonant continuum for a correct description of ultrafast processes.

*Corresponding author. georges@danaos.physics.upatras.gr

[1] T. Hertel, E. Knoesel, M. Wolf, and G. Ertl, Phys. Rev. Lett. **76**, 535 (1996).
[2] H. Petek and S. Ogawa, Prog. Surf. Sci. **56**, 239 (1997).
[3] M. J. Weida, S. Ogawa, H. Nagano, and H. Petek, Appl. Phys. A: Mater. Sci. Process. **71**, 553 (2000).
[4] M. J. Weida, S. Ogawa, H. Nagano, and H. Petek, J. Opt. Soc. Am. B **17**, 1443 (2000).
[5] J. Lehmann, M. Merschdorf, W. Pfeiffer, A. Thon, S. Voll, and G. Gerber, Phys. Rev. Lett. **85**, 2921 (2000).
[6] Y.-H. Liau, A. N. Unterreiner, Q. Chang, and N. F. Scherer, J. Phys. Chem. B **105**, 2135 (2001).
[7] M. Bauer and M. Aeschlimann, J. Electron Spectrosc. Relat. Phenom. **124**, 225 (2002).
[8] M. Sakaue, T. Munakata, H. Kasai, and A. Okiji, Phys. Rev. B **68**, 205421 (2003).
[9] C. Timm and K. H. Bennemann, J. Phys.: Condens. Matter **16**, 661 (2004).
[10] V. P. Zhukov, O. Andreyev, D. Hoffmann, M. Bauer, M. Aeschlimann, E. V. Chulkov, and P. M. Echenique, Phys. Rev. B **70**, 233106 (2004).
[11] A. Monnich, J. Lange, M. Bauer, M. Aeschlimann, I. A. Nechaev, V. P. Zhukov, P. M. Echenique, and E. V. Chulkov, Phys. Rev. B **74**, 035102 (2006).
[12] H. Ueba and B. Gumhalter, Prog. Surf. Sci. **82**, 193 (2007).
[13] N. E. Karatzas and A. T. Georges, Opt. Commun. **81**, 479 (2006).
[14] Jianming Dai, H. Teng, and Chunlei Guo, Opt. Commun. **252**, 173 (2005).
[15] P. Dombi, F. Krausz, and G. Farkas, J. Mod. Opt. **53**, 163 (2006).
[16] A. T. Georges and N. E. Karatzas, Appl. Phys. B: Lasers Opt. **81**, 479 (2005).
[17] T. Brabec and F. Krausz, Phys. Rev. Lett. **78**, 3282 (1997).
[18] A. T. Georges, Phys. Rev. A **66**, 063412 (2002).
[19] N. W. Ashcroft and N. D. Mermin, *Solid State Physics* (Saunders, Philadelphia, 1976).
[20] P. Dombi, A. Apolonski, Ch. Lemell, G. G. Paulus, M. Kakehata, R. Holzwarth, Th. Udem, K. Torizuka, J. Burgdörfer, T. W. Hänsch, and F. Krausz, New J. Phys. **6**, 39 (2004); A. Apolonski, P. Dombi, G. G. Paulus, M. Kakehata, R. Holzwarth, Th. Udem, Ch. Lemell, K. Torizuka, J. Burgdörfer, T. W. Hänsch, and F. Krausz, Phys. Rev. Lett. **92**, 073902 (2004).
[21] J. B. Smith and H. Ehrenreich, Phys. Rev. B **25**, 923 (1982).
[22] W. S. Fann, R. Storz, H. W. K. Tom, and J. Bokor, Phys. Rev. B **46**, 13592 (1992).
[23] Z. Cheng, A. Furbach, S. Sartania, M. Lenzner, Ch. Spielmann, and F. Krausz, Opt. Lett. **24**, 247 (1998).
[24] K. Yamane, T. Kito, R. Morita, and M. Yamashita, Opt. Express **12**, 2762 (2004).
[25] G. Stibenz, C. Ropers, Ch. Lienau, Ch. Warmuth, A. S. Wyatt, I. A. Walmsley, and G. Steinmeyer, Appl. Phys. B: Lasers Opt. **83**, 511 (2006).
[26] P. Lazic, V. M. Silkin, E. V. Chulkov, P. M. Echenique, and B. Gumhalter, Phys. Rev. B **76**, 045420 (2007).
[27] V. Roudnev and B. D. Esry, Phys. Rev. Lett. **99**, 220406 (2007).
[28] E. Cormier and P. Lambropoulos, Eur. Phys. J. D **2**, 15 (1998).
[29] A. T. Georges, Phys. Rev. B **51**, 13735 (1995).